Superconductivity of Li doped BSCCO mesoscopic fiber

Xian-Lin Zeng[1,*] **, Alex Wiederhold**[1]**, Michael R Koblischka**[2]**, Di Wang**[3]**, Mohammed Hammad Fawey**[3,4] **and Uwe Hartmann**[1]

[1] Institute of Experimental Physics, Saarland University, PO Box 151150, 660041 Saarbrücken, Germany
[2] Shibaura Institute of Technology Koto-ku, Tokyo, Japan
[3] Institut für Nanotechnologie, Karlsruher Institut für Technologie (KIT), Eggenstein-Leopoldshafen D-76344, Germany
[4] Physics Department, Faculty of Science, Sohag University, 82524 Sohag, Egypt

E-mail: x.zeng@physik.uni-saarland.de

Abstract

Mesoscopic Li doped BSCCO fibres are synthesized by the electrospinning technology and the sequent sintering treatment. With the assistance of high resolution energy-dispersive x-ray spectroscopy detector in the Aberration-corrected transmission electron microscopy, we discovered hidden CuO grains and separated Bi-2212 phases, which is proved by the existence of fishtail effect in the magnetization loops. The electric measurement is fulfilled via four probe method with the help of focus ion beam operation. A non-trivial resistance behaviour appears, which can be attributed to its polycrystalline and superconducting phase separation features.

Supplementary material for this article is available online

(Some figures may appear in colour only in the online journal)

1. Introduction

To fulfil wider application of the superconducting fibres, researchers have never stopped their effort on understanding the electrical mechanism of the superconducting fibres as well as their sensing application [1–4]. Especially for the superconducting nanowires, initiating from the Langer–Ambegaokar–McCumber–Halperin theory [5, 6], theoretical work based on the thermally activated phase slip and quantum tunnelling theory has been proposed to describe the electric properties of the superconducting nanowires [7, 8]. With the development of nanotechnology, experimental reports appear as proof of the theoretical prediction and demonstrate the influence of the thermal and quantum fluctuation onto the superconductivity of the nanowires [9–11].

Similar as two dimensional thin films [15–18], superconductivity of granular superconductors is of great interest to one dimensional nanowires [21, 22]. The combination of sol-gel growth method and electrospinning technology [19, 20] enables the facile preparation of superconducting polycrystalline nanowires. Recently, the superconductivity of the Bi-2212 nanowire network has been reported [23–26]. Unlike the trivial bulk Bi-2212 material, the nanowire network presents some unique feature in its electrical properties such as double resistance steps behaviour in the resistance–temperature curves and the anti-proximity effect.

As a comparison, the mesoscopic fibres attract less attention currently, let alone the single fibre. The main reason is that as the diameter of the fibre reaches micrometer scale, the size of the fibre is sufficiently large to provide the regime for flux pinning and the existence of cooper pairs. The electric properties of certain fibres should have no obvious difference from

---

* Author to whom any correspondence should be addressed.

the bulk materials. The influence of the thermal fluctuation weakens significantly when the size of the sample is micrometer scale, and the quantum phase slip appears even when the diameter of the fibre is comparable with the coherent length, which is 3–5 nm scale. The electric properties of the single superconducting nanowire has been reported [9–11], the measurement was achieved by shaping the superconducting thin film into nanowire. There have been limited accounts detailing the assessment of free-standing individual nanowires. Despite the mesoscopic fibre's dimensions being larger than those of the nanowire, although it might appear to be an insignificant subject, there has been a scarcity of studies addressing such individual microfibres as well.

In this paper, we are going to fill this vacancy of superconducting fibre research. We focus on the phase characterization and superconductivity measurement of the single polycrystalline Bi-2212 fibre, which diameter is around 1 μm. To retain the fibre's extended length, which proves advantageous for establishing electrical measurements, we introduced Li doping into the synthesis process to lower the required thermal treatment temperature [12–14]. Building upon our previous research, we found that a 30% Li doping concentration effectively accomplishes our objective [25]. Surprisingly, the electrospun polycrystalline fibre is not as simple as expected. A phase separation is discovered. Meanwhile the electric behaviour of the single fibre is also not as trivial as the bulk superconductor. An approach of single fibre measurement is introduced. The phase separation can be found via the energy-dispersive x-ray spectroscopy (EDX) detector of the transmission electron microscopy, the magnetization loops provide an agreement with this result. Furthermore, a nontrivial electric behaviour is presented in the resistance temperature measurement.

2. Experimental

To formulate the precursor necessary for the electrospinning procedure, a combination of bismuth acetate (Bi(OOCCH$_3$)$_2$)), strontium acetate hydrate (Sr(OOCCH$_3$)$_2$·xH$_2$O), calcium acetate hydrate (Ca(OOCCH$_3$)$_2$·xH$_2$O), copper acetate hydrate (Cu(OOCCH$_3$)$_2$·H$_2$O), and lithium acetate Li(OOCCH$_3$) was amalgamated in a designated proportion of Bi:Sr:Ca:Li:Cu = 2:2:2:1.2:2.8. All of these chemicals are conveniently procurable from Alfa Aesar GmbH and Co KG, boasting a purity level surpassing 99.99%. The ratio 0.3:0.7 of Li to Cu is chosen to obtain the doping level of 30% Li and the excessive Ca and Cu are applied to suppress the impurity formation [27]. The compounds were solved in propionic acid and polyvinylpyrrolidone (PVP) was added in order to obtain an adequate viscosity.

The electrospinning was performed with a MECC nanofibre electrospinner with an applied voltage of 25 V and a pump rate of 0.2 ml h^{-1} at a temperature of 28 °C. The resulting fibres were collected on a cut silicon substrate.

Thanks to the Li doping the maximum sintering temperature was reduced from around 800 °C to 750 °C. The

temperature reduction effectively prevents the fibres from collapse during the annealing process. Meanwhile, the fibres obtain superconducting Bi-2212 phase at this lower temperature. The rest of the sintering steps are the same as in our former work with nanowire [25].

The sample preparation for electric measurements was carried out employing focus ion beam technique (FIB, FEI Strata 400 STEM) on single fibre transportation. Before the thermal treatment some scratches are applied to the as prepared fibre network. During the heat process, the edges of the scratch tilt due to surface tension. In this way, more long, free standing fibres can be found, which is convenient for the later approach of the FIB manipulator. The transport procedure is shown in figure 1. The fibre is transported to the gold electrode pattern of the lithographically produced sample holder. With an applied force by the manipulator, no gap appears between the fibre and the electrode. It provides good conductive connection on such junctions. Finally, platinum is deposited to fix the contacts. In contrast to the standard procedure in FIB, which uses the ion beam, here, the electron beam was used for the deposition, in order to reduce the platinum contamination into the superconducting fibre. This was repeated for all four electrodes. The fully contacted fibre is shown in figure 1(d). After this procedure, the substrate was glued on a PCB socket and connected in a way, which allows the four wire measurement.

The microstructure was observed by means of scanning electron microscopy (SEM, Hitachi S800) and Aberration-corrected transmission electron microscopy (Cs-TEM, FEI Titan 80-300). The magnetic properties were measured in the physics properties measurement system (PPMS, QuantumDesign) and the electrical measurement was performed within an Oxford Teslatron Cryostat together with a Keithley 2400 source meter in four-wire sensing mode.

3. Result and discussion

3.1. Microstructure

Figure 2(a) presents the polycrystalline microstructure of the Bi-2212 fibres after thermal treatment in SEM observation. The average length of the fibres is in the range of hundred micrometers, while the diameter of the fibre is around 1 μm as shown in figure 2(b) and the mean grain size is around 300 nm, corresponding to the TEM observation in figure 2(c). Figure 2(d) shows the lattice information from a segment of the grain. It is well-orientated in uniform direction except a small distortion shown in figure 2(e). It indicates that the crystallization quality of the fibre is good, however, there are defects inside the grain, which can serve as pinning centre of the whole fibre.

3.2. Phase characterization

According to our former work with x-ray diffraction (XRD) analysis [25], with 30% Li doping, the nanowire network contains two phases: Bi-2212 as the main phase and Bi-2201
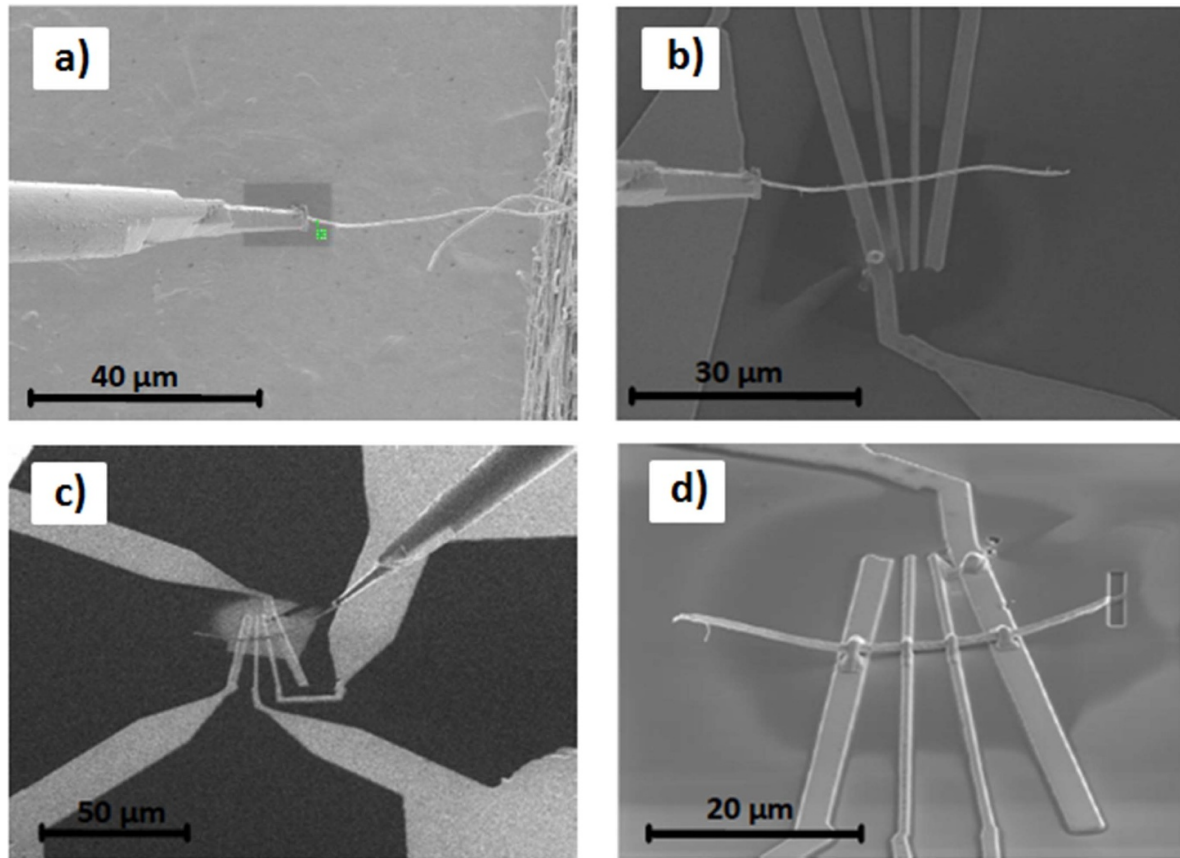
Figure 1. FIB transportation of the single fibre. A single fibre is fixed onto the micromanipulator by platinum deposition (a). After that, it is moved towards the lithographically produced electrode pattern (b). A bending of the fibre towards the electrodes enables to obtain a suitable contacting (c), which is obtained via platinum deposition. The fully contacted fibre is shown in (d).

as impurity phase. No evidence of the presence of Li compounds within the fibre has emerged, whether through XRD or EDAX analysis in TEM. Nonetheless, we speculate that there might be fibres with dispersed Li in the sample, potentially in the form of Li_2O. The limitation of XRD and EDAX techniques could be the reason we have yet to detect these instances. From the former TEM observation and the EDX indexing, the element distributions of the chosen grains have good agreement with the Bi-2212 phase, no Bi-2201 contribution was found. Deeper analysis is given in this work via the high resolution EDX detector in the Cs-TEM. With the spot size of around 1 nm for the detector, it enables to analysize the element distribution on individual grains of the fibres. Table I (in supplementary file) presents the element distribution of the individual grains on two chosen fibres. Some features can be found from the data:

(a) The coexistence of the Bi-2212 phase and Bi-2201 phase within a singular fibre is absent. The elemental composition ratios for Grain1 and Grain3 within fibre1 stand at Bi:Sr:Ca:Cu:O = 2.29:2.01:0.83:1.91:8.59 and Bi:Sr:Ca:Cu:O = 2.08:1.66:1.35:2.01:9.85, respectively. Both of these ratios harmonize with the anticipated proportions for the Bi-2212 phase. Conversely, the composition

ratio of Grain1 within fibre2 equates to Bi:Sr:Ca:Cu:O = 2.03:2.06:0.20:0.81:4.91, aligning with the characteristics of the Bi-2201 phase;

(b) CuO is present in grains within both types of fibres, even though trace amounts of CuO are not discernible in XRD analyses. This observation implies a distinct phase separation within the fibres, where they are partitioned into either the Bi-2212 phase along with CuO or the Bi-2201 phase alongside CuO;

(c) The oxidization level differs in various Bi-2212 grains within one single fibre. As it can be seen from Grain1 and Grain3 in fibre1. The element ratio of O in Grain1 is 8.59 while the value is higher in Grain3, which is 9.85.

The features showcased herein are not an isolated observation. In fact, we have encountered analogous instances in several grains situated within distinct fibres. However, it is important to note that we have not examined all the fibres within our preparations, resulting in somewhat limited statistical coverage. From the analysis above, the measurement on the fibre with Bi-2212 phase is not influenced by the Bi-2201 phase. However, the influence from CuO and different oxidization levels cannot be ignored.
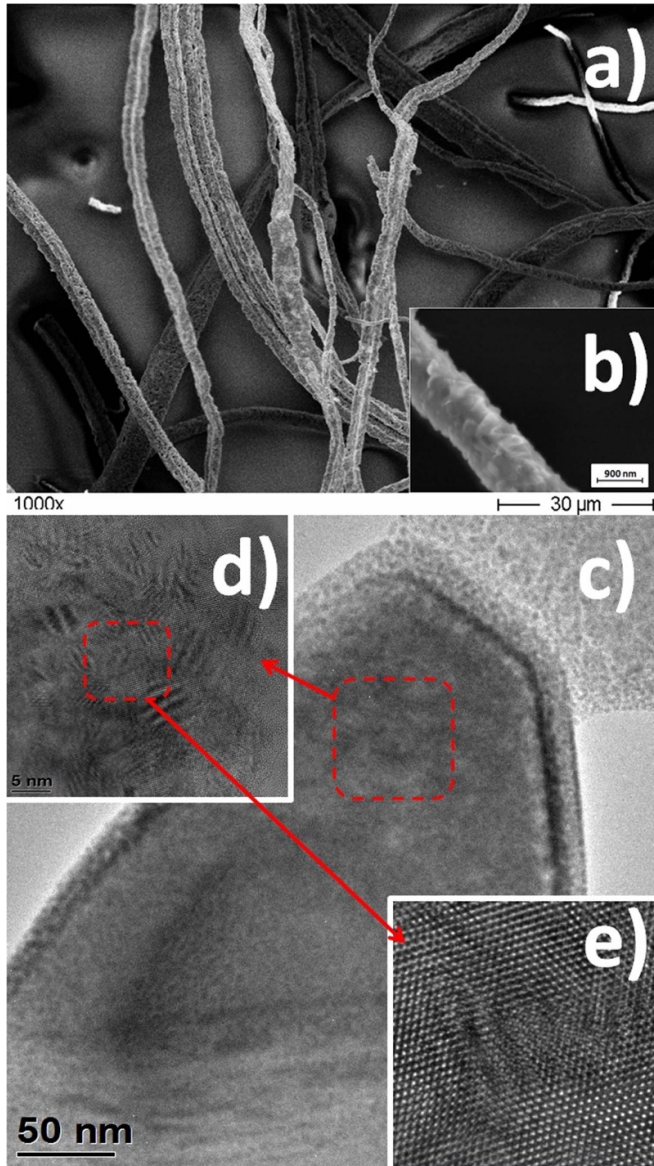
Figure 2. Microstructure of the Bi-2212 fibres after thermal treatment. (a) SEM image of the Bi-2212 fibres with magnification ×1000 (b) high resolution SEM image of a single Bi-2212 fibre, (c) TEM observation on one grain of the single fibre, (d) lattice orientation of the grain (e) zoom-in detail of the atomic arrangement.

3.3. Magnetic properties

For the superconducting nanowires, the superconductivity is suppressed by the thermal fluctuation and quantum fluctuation [7, 8]. With larger diameter, the mesoscopic fibre experiences less size suppression. It can provide more regime for the existence of carrier cooper pairs, meanwhile, the influence from thermal fluctuation is not as obvious as in nanowire system. The mesoscopic fibre should present better superconductivity than the nanowire. Figure 3 presents the magnetic properties of the Bi-2212 fibre. As expected, the mesoscopic fibre shows higher T_c (86.2 K, the T_c of the Li doped

Bi-2212 nanowire is around 74 K [25]) in the zero field cooling $M(T)$ curve. Figure 3(a) presents the $M(H)$ loops of the sample at 10 and 20 K. There is no obvious paramagnetic background as in nanowire system. It denotes that the signal from the superconducting component in the fibre are strong enough to suppress the potential magnetic signal from the CuO grains.

On the other hand, the magnetization loops of the mesoscopic fibre exhibit distinctions from the conventional superconducting hysteresis patterns. Notably, an arch-shaped feature becomes apparent in the high-field region, as depicted in the inset $\Delta M(H)$ plot of figure 3(a). At 10 K, a distinct turing of ΔM ($M(H_{decreasing}) - M(H_{increasing})$) becomes evident at approximately $x = 5$ T. For the 20 K dataset, a comparable turning phenomenon appears at around $x = 5.5$ T. In the standard scenario, the magnetization curve within these domains is anticipated to remain horizontally aligned with respect to the $M = 0$ axis. This is called the fishtail effect. A similar phenomenon has been observed in non-doped Bi-2212 nanowires and Pb-doped Bi-2212 nanowires [24]. However, in the case of the mesoscopic fibre, this effect emerges at a higher field and over a broader range. This phenomenon indicates an underlying increase of pinning at high field, which could be ascribed to the transition of vortex lattice [28] or phase separation [29]. The order-disorder transition of the vortex lattice mainly happens when the temperature approaches T_c, therefore, it does not coincide with our case that the fishtail effect is stronger at 10 K rather than at 20 K. Recalling the result from EDX analysis, the grains in the Bi-2212 fibre can be classified into three types: CuO grains; weakly oxidized Bi-2212 grains and highly oxidized Bi-2212 grains. The superconducting phase is separated by different oxidization levels. It is plausible to consider that the fishtail effect here is an evidence of the phase separation in the Bi-2212 mesoscopic fibre.

3.4. Electric properties

Figure 4 illustrates the temperature-dependent resistance ($R(T)$) measurement conducted on an individual mesoscopic Bi-2212 fibre with an applied current of 50 nA. In its normal state, the fibre's conductive characteristics more closely resemble those of a semiconductor rather than a metal, deviating from the behaviour exhibited by the bulk material. The fibre's resistance is notably high, lying within the order of $\times 10^7 \Omega$. The contact interface area between the fibre and the electrode remains confined to less than 1 μm^2. Consequently, this pronounced resistance can be predominantly attributed to the weak electrical connection between the fibre and the electrode. Even with platinum deposition, the dominant contribution to the overall system resistance persists as high-value interface junction resistances.

As the temperature decreases, the electric behaviour of the single fibre is not as trivial as the bulk superconductor. The initial reduction in resistance becomes evident around 95 K, followed by a subsequent decline at approximately
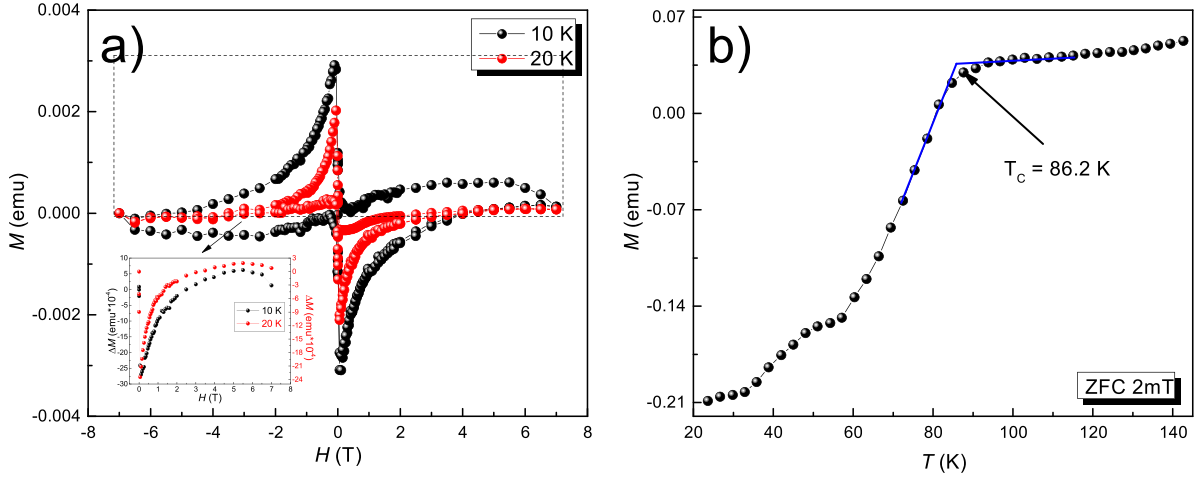
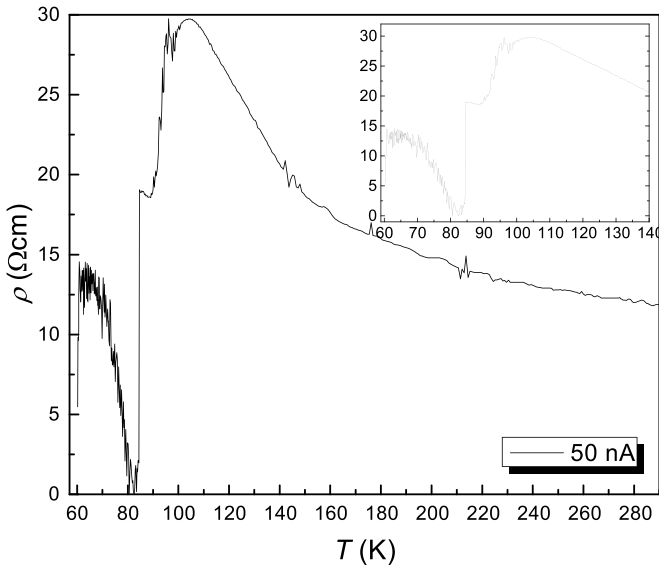**Figure 3.** Magnetic properties of the Bi-2212 fibres via PPMS.

Figure 4. The $R(T)$ measurement of the Bi-2212 fibre with applied current 50 nA.

86 K, which corresponding to the T_c estimation from the magnetic data. Since the Schottky connection cannot provide resistance reduction with decreasing temperature, the observed resistance behaviour within this range arises solely from the intrinsic electrical properties of the fibre.

Just below T_c, at around 83 K, the resistance displays an upward trend as the temperature drops, persisting until approximately 65 K. In this temperature interval, the superconductivity within the fibre is suppressed by the growing resistance emanating from the Schottky connection between the fibre and electrodes.

Unfortunately, the pursuit of resistance measurements at lower temperatures encounters obstruction due to high-frequency noise originating from the source meter and multimeter. Drawing from insights gained through experiences with the Li-doped Bi-2212 nanowire network system, it is anticipated that the resistance will decrease but will not reach a null value.

Within the temperature span of approximately 95 K to 83 K, the observed electrical behaviour has not been found in the bulk or thin film system. In our former work, the polycrystalline nanowire network presents a double resistance drop behaviour. However, the resistance drop at above 90 K has never been discovered in our nanowire system. The possible mechanism of the single mesoscopic fibre may be hidden from its polycrystalline structure and the phase separation feature.

According to the report from Boulesteix *et al* [30], the T_c of the Bi-2212 crystal is strongly related to the dependence on the excess of oxygen atoms in the BiO layers, meanwhile when the current passes through the BiO layer, the resistance behaviour can be separated into metallic behaviour and semiconducting behaviour, depending on the current is in-plane or out-of-plane of the layer. Taking account of our Bi-2212 fibre system, the polycrystalline structure provides the possibility of the applied current passing through grains with various orientation to their BiO layers; the Bi-2212 grains with high oxidization level enter superconducting state at higher temperature, while the weak oxidization ones become superconducting at lower temperature. The non-trivial electric behaviour of the single fibre can be attributed to the combination of these properties. As shown in figure 5, when current passes through three different types of Bi-2212 grains, the electric behaviour is demonstrated by the black, red and green plots respectively. A summarized curve is presents in blue plot. It has a good agreement with the resistance drop feature of the single fibre. Combined with the semiconducting contribution from the CuO grains, we find a suitable explanation to the electric behaviour of our single fibre.

4. Conclusions

In this paper, we introduce an approach of investigating the superconductivity of the polycrystalline mesoscopic Bi-2212 fibre. With the assistance of the high-resolution EDX detector
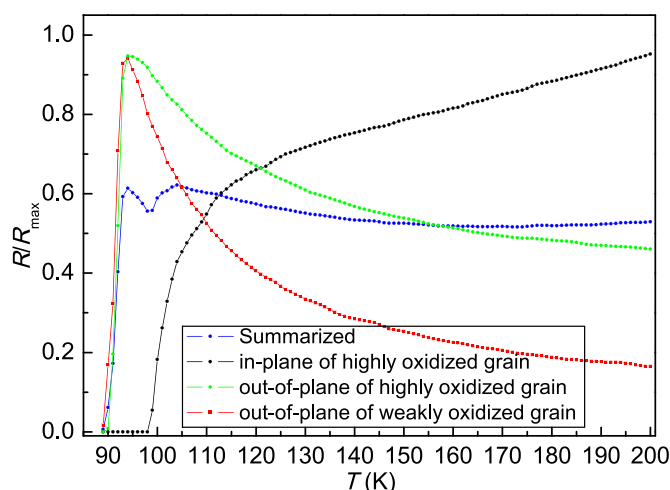
Figure 5. The $R(T)$ behaviours of Bi-2212 crystal grains [30]: black dots curve represents the $R(T)$ curve of the highly oxidized grain with current passing through in-plane; green dots curve represents the $R(T)$ curve of the highly oxidized grain with current passing through out-of-plane; the red one represents the $R(T)$ curve of the weakly oxidized grain with current passing through out-of-plane; blue dots curve is a summarise of all the cases.

within the Cs-TEM, we have successfully unveiled concealed CuO grains and distinct phases of superconducting Bi-2212. The $M(T)$ measurement confirms the superconductivity of the fibre, and the T_c of the fibre is higher than the nanowire system. The fishtail effect is found in the magnetization loops, which proves the existence of the superconducting phase separation. A non-trivial resistance behaviour appears in the electric measurement. The resistance drops stepwise with decreasing temperature. The first drop appears at ∼95 K, the second one appears at ∼86 K, and the last resistance decrease appears at ∼65 K before the end of the measurement. The behaviour of applied current passing through three types of grains in the Bi-2212 fibre has a good agreement with such behaviour. In other words, the specific electric properties of the mesoscopic Bi-2212 fibre stem from its polycrystalline and phase separation features.

Within the scope of our restricted statistical framework, the discovered features unveiled through the EDX data can be universally applied to the observed fibres. Furthermore, the manifestation of fishtail effect within the magnetization curve originates from the large amount of samples, where the electrical characteristics of a single fibre encompass all grains within that fibre. These two findings collectively point to a scenario of phase separation. Hence, we are inclined to posit that the existence of phase separation, indicative of oxygen level discrepancies, persists within our fibres, despite deviations from the oxygen ratios presented above. On a divergent note, localized variations in oxygen content during thermal treatment are a customary occurrence in ceramic oxides. Although seldom invoked as an explanation due to its limited influence on the magnetic and electrical properties of the sample, our comprehensive analysis combining EDX, magnetization, and electrical measurements leads us to favour a more credible

interpretation: the phase separation attributed to non-uniform oxygen distribution within the grains.

Data availability statement

No new data were created or analysed in this study.

Conflict of interest

There are no conflicts to declare.

ORCID iDs

Xian-Lin Zeng ⓘ https://orcid.org/0000-0002-1937-4358
Uwe Hartmann ⓘ https://orcid.org/0000-0002-6986-9092

References

[1] Natarajan C M, Tanner M G and Hadfield R H 2012 Superconducting nanowire single-photon detectors: physics and applications *Supercond. Sci. Technol.* **25** 063001
[2] You L 2020 Superconducting nanowire single-photon detectors for quantum information *Nanophotonics* **9** 2673–92
[3] Korzh B *et al* 2020 Demonstration of sub-3 ps temporal resolution with a superconducting nanowire single-photon detector *Nat. Photon.* **14** 250–5
[4] Steinhauer S, Gyger S and Zwiller V 2021 Progress on large-scale superconducting nanowire single-photon detectors *Appl. Phys. Lett.* **118** 100501
[5] Langer J S and Ambegaokar V 1967 Intrinsic resistive transition in narrow superconducting channels *Phys. Rev.* **164** 498
[6] McCumber D E and Halperin B I 1970 Time scale of intrinsic resistive fluctuations in thin superconducting wires *Phys. Rev.* B **1** 1054
[7] Lukens J E, Warburton R J and Webb W W 1970 Onset of quantized thermal fluctuations in "one-dimensional" superconductors *Phys. Rev. Lett.* **25** 1180–3
[8] Newbower R S, Beasley M R and Tinkham M 1972 Fluctuation effects on the superconducting transition of tin whisker crystals *Phys. Rev.* B **5** 864–8
[9] Bezryadin A, Lau C N and Tinkham M 2000 Quantum suppression of superconductivity in ultrathin nanowires *Nature* **404** 971–4
[10] Tian M, Wang J, Kurtz J S, Liu Y, Chan M H W, Mayer T S and Mallouk T E 2005 Dissipation in quasi-one-dimensional superconducting single-crystal Sn nanowires *Phys. Rev.* B **71** 104521
[11] Altomare F, Chang A M, Melloch M R, Hong Y and Tu C W 2006 Evidence for macroscopic quantum tunneling of phase slips in long one-dimensional superconducting Al wires *Phys. Rev. Lett.* **97** 017001

[12] Kawai T, Horiuchi T, Mitsui K, Ogura K, Takagi S and Kawai S 1989 Effect of alkaline metal substitutions to Bi-Sr-Ca-Cu-O superconductor *Physica* C **161** 561–6

[13] Volkov M P, Melekh B T, Bakharev V I, Kartenko N F, Matykin N V and Filin Y N 1999 Effect of Li doping on the critical temperature and glass formation in the Bi-Sr-Ca-Cu-O system *Phys. Solid State* **41** 15–17

[14] Khalil S M 2007 Influence of alkaline metal Li1+ intercalation on the excess conductivity, thermopower and hardness of BSCCO pellets *Physica* B **391** 130–5

[15] Pearl J 1964 Current distribution in superconducting films carrying quantized fluxoids *Appl. Phys. Lett.* **5** 65–66

[16] Kosterlitz J M and Thouless D J 1973 Ordering, metastability and phase transitions in two-dimensional systems *J. Phys. C: Solid State Phys.* **6** 1181–203

[17] Beasley M R, Mooij J E and Orlando T P 1979 Possibility of vortex-antivortex pair dissociation in two-dimensional superconductors *Phys. Rev. Lett.* **42** 1165–8

[18] Mironov A Y, Silevitch D M, Proslier T, Postolova S V, Burdastyh M V, Gutakovskii A K, Rosenbaum T F, Vinokur V V and Baturina T I 2018 Charge Berezinskii-Kosterlitz-Thouless transition in superconducting NbTiN films *Sci. Rep.* **8** 4082

[19] Ding B, Kim H-Y, Lee S-C, Shao C-L, Lee D-R, Park S-J, Kwag G-B and Choi K-J 2002 Preparation and characterization of a nanoscale poly(vinyl alcohol) fiber aggregate produced by an electrospinning method *J. Polym. Sci.* B **40** 1261–8

[20] Mai L, Xu L, Han C, Xu X, Luo Y, Zhao S and Zhao Y 2010 Electrospun ultralong hierarchical vanadium oxide nanowires with high performance for lithium ion batteries *Nano Lett.* **10** 4750–5

[21] Bollinger A T, Rogachev A, Remeika M and Bezryadin A 2004 Effect of morphology on the superconductor-insulator transition in one-dimensional nanowires *Phys. Rev.* B **69** 180503(R)

[22] Bar E, Levi D, Koren G, Shaulov A and Yeshurun Y 2014 Transport properties of ultra-thin granular $YBa_2Cu_3O_{7-\delta}$ nanobridges *Physica* C **506** 160–4

[23] Koblischka M R, Zeng X L, Karwoth T, Hauet T and Hartmann U 2016 Transport and magnetic measurements on $Bi_2Sr_2CaCu_2O_8$ nanowire networks prepared via electrospinning *IEEE Trans. Appl. Supercond.* **26** 1800605

[24] Zeng X L, Koblischka M R, Karwoth T, Hauet T and Hartmann U 2017 Preparation of granular Bi-2212 nanowires by electrospinning *Supercond. Sci. Technol.* **30** 035014

[25] Zeng X L, Koblischka M R, Laurent F, Karwoth T, Koblischka A V, Hartmann U, Chang C, Kumar P and Eibl O 2018 Characterization of electrospun $Bi_2Sr_2CaCu_2O_{8+\delta}$ nanowires with reduced preparation temperature *IEEE Trans. Appl. Supercond.* **28** 1–5

[26] Koblischka M R, Koblischka A V, Zeng X L, Hannachi E and Slimani Y 2020 Microstructure and fluctuation-induced conductivity analysis of $Bi_2Sr_2CaCu_2O_{8+\delta}$ (Bi-2212) nanowire fabrics *Crystals* **10** 986

[27] Schwartz J and Wu S 1991 Effects of lithium doping on the formation and microstructure of bulk Bi-Sr-Ca-Cu-O *Physica* C **190** 169–71

[28] Mikitik G P and Brandt E H 2001 Peak effect, vortex-lattice melting line and order-disorder transition in conventional and high-T_C superconductors *Phys. Rev.* B **64** 184514

[29] Nakamura M, Yamada Y, Hirayama T, Ikuhara Y, Shiohara Y and Tanaka S 1996 Heat treatment and anomalous peak effect in $J_C - H$ curve at 77 K for $NdBa_2Cu_3O_{7-\delta}$ single-crystal superconductor *Physica* C **259** 295–303

[30] Boulesteix C, Marietti Y, Badéche T, Tatarenko-Zapolsky H, Grachev V, Monnereau O, Faqir H and Vacquier G 2000 Use of out-of-plane resistivity for determination of the 2D or 3D character of superconductive fluctuations for Bi-2212 crystals in the mixed state and origin of anomalous high out-of-plane resistivity for weakly oxidized crystals *J. Phys. Chem. Solids* **61** 585–92